Biosensors and Bioelectronics 100 (2018) 462–468

Contents lists available at ScienceDirect

Biosensors and Bioelectronics

journal homepage: www.elsevier.com/locate/bios

Electrophysiological investigation of human embryonic stem cell derived neurospheres using a novel spike detection algorithm

Margot Mayer[a,*], Onetsine Arrizabalaga[b], Florian Lieb[c], Manuel Ciba[a], Sylvia Ritter[b], Christiane Thielemann[a]

[a] University of Applied Sciences Aschaffenburg, BioMEMS Lab, Würzburger Str. 45, 63743 Aschaffenburg, Germany
[b] GSI Helmholtz Centre for Heavy Ion Research, Biophysics division, Planckstr. 1, 64291 Darmstadt, Germany
[c] University of Applied Sciences Aschaffenburg, Department of Technomathematics, Würzburger Str. 45, 63743 Aschaffenburg, Germany

ARTICLE INFO

Keywords:
Microelectrode array
Neurosphere
Spike detection algorithm
Human embryonic stem cell-derived neurons
SWTTEO
3D culture

ABSTRACT

Microelectrode array (MEA) technology in combination with three-dimensional (3D) neuronal cell models derived from human embryonic stem cells (hESC) provide an excellent tool for neurotoxicity screening. Yet, there are significant challenges in terms of data processing and analysis, since neuronal signals have very small amplitudes and the 3D structure enhances the level of background noise. Thus, neuronal signal analysis requires the application of highly sophisticated algorithms. In this study, we present a new approach optimized for the detection of spikes recorded from 3D neurospheres (NS) with a very low signal-to-noise ratio. This was achieved by extending simple threshold-based spike detection utilizing a highly sensitive algorithm named SWTTEO. This analysis procedure was applied to data obtained from hESC-derived NS grown on MEA chips. Specifically, we examined changes in the activity pattern occurring within the first ten days of electrical activity. We further analyzed the response of NS to the GABA receptor antagonist bicuculline. With this new algorithm method we obtained more reliable results compared to the simple threshold-based spike detection.

1. Introduction

The cultivation of neuronal cells on microelectrode array (MEA) chips is an established method to investigate neuronal network communication (Ben-Ari, 2001; Pine, 1980; Wagenaar et al., 2006). MEA chips have been widely used to characterize the spontaneous (Chiappalone et al., 2006; Mazzoni et al., 2007) and the evoked activity of neuronal networks (Brewer et al., 2009; Wagenaar et al., 2005) and emerge as an important tool for neurotoxicity screening (Johnstone et al., 2010).

Although *in vivo* and *in vitro* animal models have contributed much to our knowledge about neuronal network communication their use in predicting the effect of neuroactive substances is limited. Past experience showed that several substances are teratogenic in animal models but not in humans (*e.g.* aspirin (Klein et al., 1981)) and *vice versa* (*e.g.* thalidomide (Lepper et al., 2006)). For this reason, human cell models are highly desirable for toxicological studies. For a long time, the constraining factor has been the availability of suitable *in vitro* systems. However, due to the progress in stem cell research, human embryonic stem cells (hESC) have the capability of unlimited proliferation *in vitro* without losing their potential to differentiate into derivatives of all three germ layers (Thomson et al., 1998) under appropriate growth conditions. Further, it was shown that neural differentiation of hESC faithfully recapitulate early developmental processes *in vivo* (Colleoni et al., 2011; Zimmer et al., 2012), making them highly suitable as an *in vitro* model to assess developmental neurotoxicity.

However, also limitations of 2D culture systems become increasingly apparent. Cells in a living organism are organized in a three-dimensional (3D) architecture that is not reflected in 2D cell models, resulting in misleading and non-predictive data for *in vivo* responses (*e.g.* reaction after exposure to the anti-cancer drug paclitaxel (Loessner et al., 2010)). Furthermore, an increasing number of studies demonstrate that 3D *in vitro* or *in vivo* systems differ from monolayer networks with respect to proliferation (Hindie et al., 2006), differentiation (Willerth et al., 2006), morphology (Weaver et al., 1997) and gene expression (Birgersdotter et al., 2005). Consequently, electrophysiological properties of cells grown in traditional 2D culture differ from those grown in 3D aggregates. These differences are not restricted to the cells in the depth of 3D aggregates; also cells of the outer surface show a different electrophysiological activity than 2D cultures as

* Corresponding author.
E-mail addresses: Margot.Mayer@h-ab.de (M. Mayer), O.ArrizabalagaDeMingo@gsi.de (O. Arrizabalaga), Florian.lieb@h-ab.de (F. Lieb), Manuel.ciba@h-ab.de (M. Ciba), S.Ritter@gsi.de (S. Ritter), Christiane.Thielemann@h-ab.de (C. Thielemann).

http://dx.doi.org/10.1016/j.bios.2017.09.034
Received 9 June 2017; Received in revised form 10 August 2017; Accepted 18 September 2017
Available online 19 September 2017

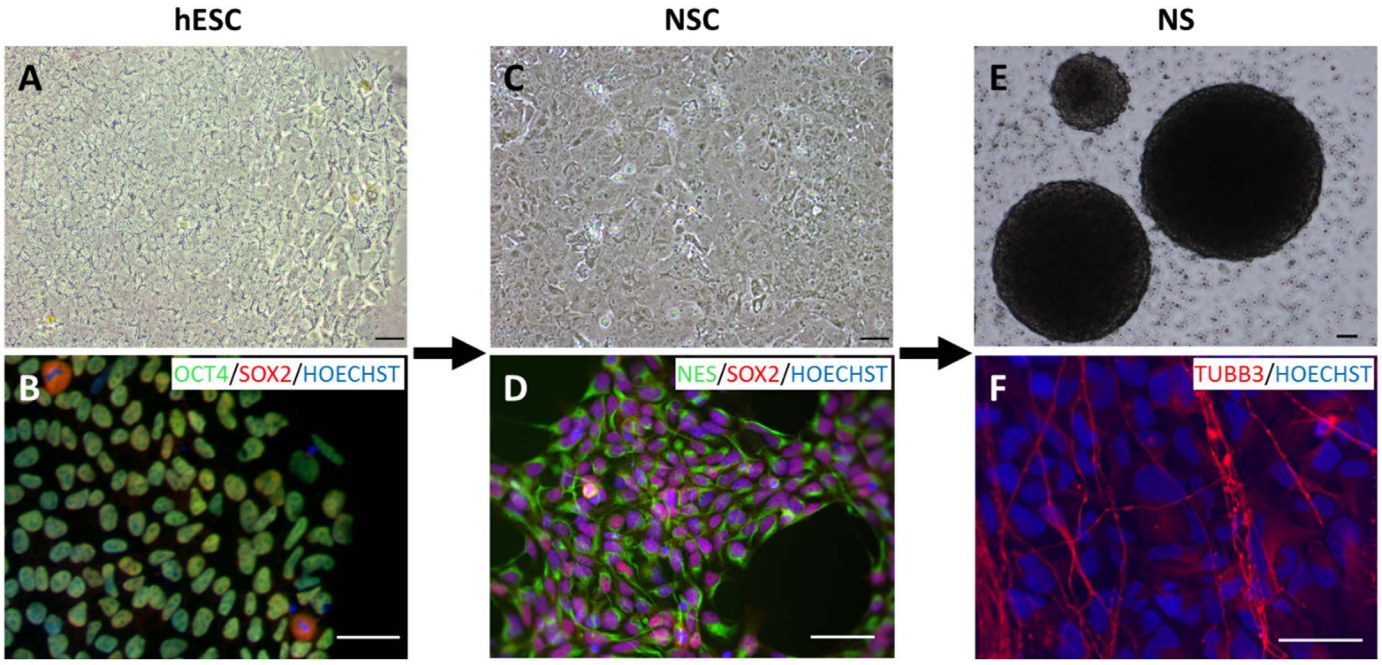

Fig. 1. Generation of hESC-derived NS. hESC were cultured on Geltrex (A). Immunofluorescence staining confirmed the presence of OCT4 (green) and SOX2 (red) in hESC cultures (B). Differentiation of hESC to NSC was efficiently performed within seven days as reflected in altered cell morphology (C). Immunostaining confirmed that NSC were positive for Nestin (green) and SOX2 (red) (D). Subsequently, NSC were enzymatically dissociated and cultured in suspension yielding NS (E). When transferred to a coverslip (or a MEA) NS attached and cells migrated radially out. Outgrowing cells were positive for the protein β-tubulin$_{III}$ indicative of a neuronal phenotype (red) (F). Nuclei were generally counterstained with Hoechst (blue). Scale bar = 50 µm. (For interpretation of the references to color in this figure legend, the reader is referred to the web version of this article.)

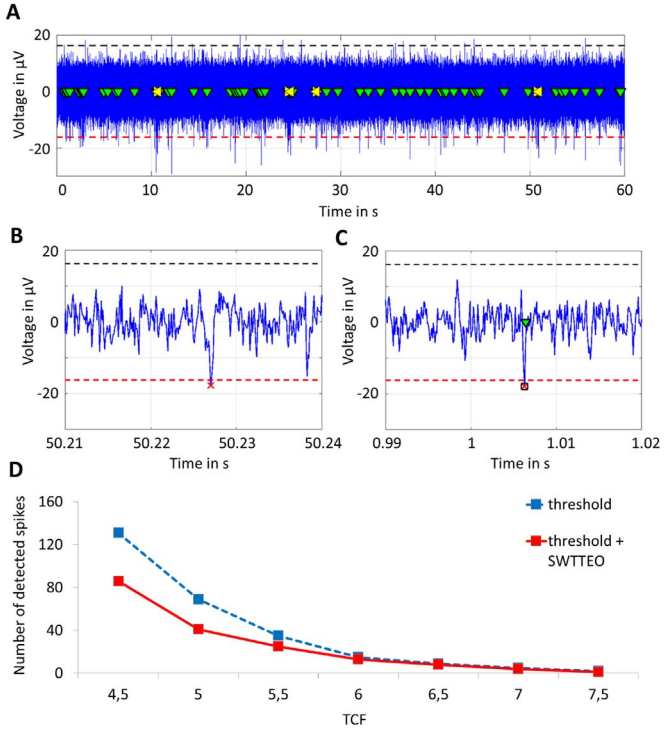

Fig. 2. The combination of a simple threshold detection with the SWTTEO algorithm lead to more reliable results. A typical neuronal measurement recorded by a single electrode. Spikes are marked with a green triangle and bursts with a yellow one (A). Data analysis is accomplished by using both, the simple threshold detection and the SWTTEO algorithm using a TCF of 4,5. Signals detected only by the threshold were marked with a red X (B). Signals that were detected by both algorithms were tagged with a square and an X (C). Only these signals are considered as spikes, marked with a green arrow. Compared with only threshold-based spike detection (blue line), the combination with SWTTEO (red line) resulted in a reduced number of detected signals using TCF < 6 (D). (For interpretation of the references to color in this figure legend, the reader is referred to the web version of this article.)

reported by Frega et al. (2014) using MEA chips with plane electrodes.

Neuronal 3D cultures derived from hESC grown on MEA chips are an ideal tool to study developmental neurotoxicity as mentioned above. Yet, there are significant challenges in terms of data processing and analysis. For example, the number of cells within the detection range of a single electrode is much higher than in 2D cell models leading to a significantly increased number of recorded signals and an enhanced level of background noise. Furthermore, electrical signals from ESC-derived neuronal cultures have very small amplitudes that hardly exceed values of 50 µV (Heikkila et al., 2009). Thus, the signal analysis requires the application of highly sophisticated algorithms. Spike detection is typically accomplished by threshold-based algorithms, defined by a multiple of noise´s standard deviation (Nick et al., 2013), where threshold calculation factors (TCF) of ≥ 5 were found in the literature. However, for the detection of signals with small amplitudes far below this threshold this approach is inadequate.

In this study, we present a novel approach for the detection of signals with small amplitudes allowing a profound reduction in the number of false positive signals. This approach is based on a new spike detection algorithm named stationary wavelet transform based teager energy operator (SWTTEO) (Lieb et al., 2017). Recent work demonstrated already the superior performance of SWTTEO in a very low signal-to-noise environment compared to other commonly used algorithms by using simulated data (Lieb et al., 2017). Yet, sole application of SWTTEO for experimental data is not applicable since the absolute number of spikes in the data set is required (as given for simulated data). To utilize SWTTEO for experimental data, it was combined with simple threshold-based spike detection and applied for the first time to experimental data obtained from hESC-derived 3D neurospheres (NS) grown on MEA chips. Specifically, we examined changes in the activity pattern occurring within the first ten days of electrical activity. We further analyzed the response of NS to the γ-aminobutyric acid (GABA) receptor antagonist bicuculline.

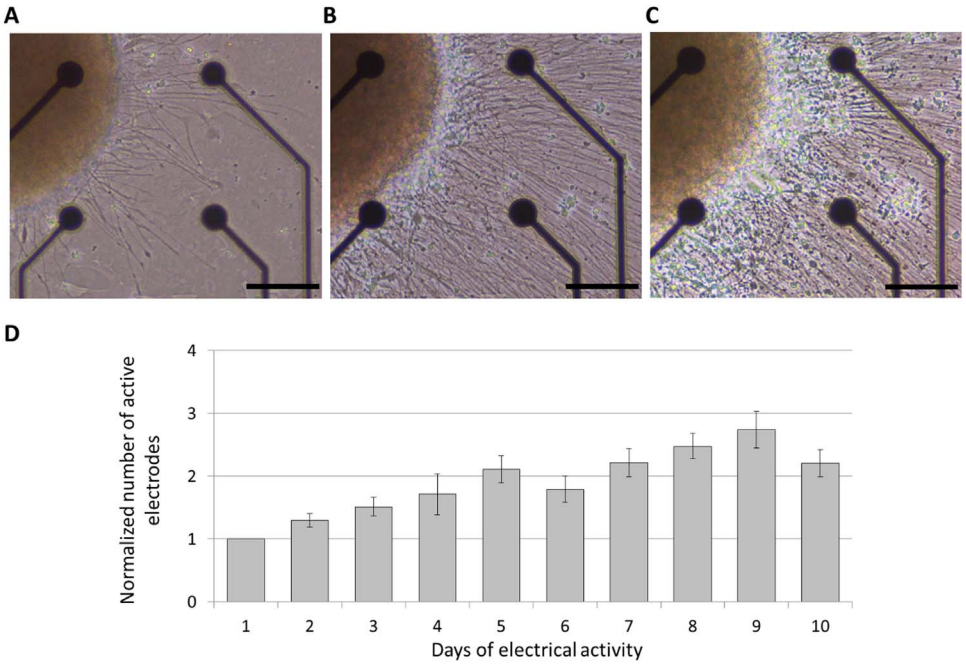

Fig. 3. hESC-derived NS form spontaneously active networks on MEA chips. NS were plated on the electrode array and cells migrated radially out over time while cell density as well as their outgrowth distance increased over time. The illustration shows the outgrowing cells on day 1 (A), day 4 (B) and day 10 (C) after plating. The number of active electrodes increased about twofold over time reflecting the outgrowth of cells (D). Data are represented as mean (n = 17) ± SEM normalized to day 1. Scale bar = 200 µm.

2. Material and methods

2.1. NSC differentiation of hESC

WA09 (H9) hESC (WiCell, Madison, USA) were differentiated into neural stem cells (NSC). Briefly, H9 cells were cultured on irradiated, mitotically inactive PMEF-NL embryonic fibroblasts (Millipore, Billerica, USA) in KnockOut™ DMEM supplemented with 20% KnockOut™ Serum Replacement (ThermoFisher Scientific, Waltham, USA), 1 mM stable glutamine (PAA Laboratories, Pasching, Austria), 1x non-essential amino acids (Biochrom, Berlin, Germany), 100 µM b-mercaptoethanol (Carl Roth, Karlsruhe, Germany), 50 U/ml penicillin and 50 µg/ml streptomycin (H9-medium). For daily feeding 10 ng/ml basic fibroblast growth factor (bFGF, Peprotech, Rocky Hill, USA) was added (for further details see (Luft et al., 2017)).

To deplete feeder cells, H9 were grown for a week on Geltrex® (ThermoFisher Scientific) coated flasks in PMEF-NL conditioned H9 medium with 4 ng/ml bFGF. Then, H9 cells were dissociated using ReLeSR™ (StemCell Technologies, Vancouver, Canada). Cell aggregates were replated on Geltrex-treated cell culture dishes at a density of 2–3 × 10^4 cells/cm^2 in conditioned H9 medium with 4 ng/ml bFGF and 5 µM ROCK Inhibitor Y-27632 (Tocris, Bristol, UK). One day after passaging neural differentiation was initiated by switching the medium to complete Gibco™ PSC neural induction medium (ThermoFisher Scientific) (Yan et al., 2013). Subsequently, neural induction medium was changed on days 2, 4 and 6 of culturing.

2.2. Neurosphere formation and analysis measurement of neurosphere diameter

At day 7 of neural induction primitive NSC were detached using Accutase™ (ThermoFisher Scientific). Cells were seeded at a density of 10^5 cells/ml onto ultra-low attachment 6 well plates (Corning, New York, USA) in NS-B27 medium (DMEM/F-12 medium, 0.5 mM Glutamine and B-27 supplement, all from ThermoFisher Scientific), supplemented with 20 ng/ml bFGF, 600 nM Dorsomorphin (Tocris) and 84 ng/ml Noggin (Peprotech) to generate NS. At day 1 of NS formation 20 µM ROCK Inhibitor Y-27632 was also added to the medium. Half of the medium was removed and fresh NS-B27 medium with supplements was added twice a week. After 18 days, NS were placed either on coverslips for immunofluorescence staining or on MEA chips for electrophysiological recording.

For quality control, the average sphere diameter was determined on day 14 after NS formation using a Nikon Eclipse TS100 microscope and the NIS-Elements documentation software (Nikon, Tokio, Japan). A total of 431 NS derived from 4 independent experiments were analyzed.

2.3. Immunocytochemistry

NS were cultured on coverslips, fixed at different developmental stages with 3.7% paraformaldehyde in PBS and processed according to standard techniques. Samples were incubated with the following primary antibodies: the pluripotent marker OCT4 (1:100, Santa Cruz Biotechnologies, Santa Cruz, USA), the pluripotent and NSC marker SOX2 (1:50, Life technologies, Carlsbad, USA), the NSC marker Nestin (1:50, Life technologies) and the neuronal marker β-tubulin$_{III}$ (1:1000, Abcam, Cambridge, UK). Secondary antibodies were: Alexa594-conjugated donkey anti-mouse (1:200, Abcam), Alexa594-conjugated donkey anti-rabbit (1:200, Life technologies) and Alexa488-conjugated donkey anti-goat (1:200, Life technologies). Nuclei were counterstained with Hoechst (ThermoFisher Scientific) and viewed under a fluorescence microscope.

2.4. Electrophysiology

Electrical activity of hESC-derived NS was examined by means of a non-invasive, *i.e.* extracellular MEA recording technique. MEA chips were obtained from Multichannel Systems (Reutlingen, Germany) and consisted of 60 titanium nitride electrodes embedded in a glass substrate and arranged in an 8 × 8 grid with an inter-electrode distance of 200 µm and an electrode diameter of 30 µm. MEA chips were coated with Polyethyleneimine (PEI, Sigma-Aldrich, St. Louis, USA) and laminin (Sigma-Aldrich). Briefly, MEA chips were filled with PEI solution (0.1% in boric acid buffer) and incubated at room temperature for one hour. Then, the solution was aspirated, chips were rinsed 4 times with sterile water and air-dried overnight. On the following day a 50 µl droplet of laminin (20 µg/ml in PBS) was applied to the array. After incubation for 1 h at 37 °C, excess laminin was removed, the cavity was filled with 1 ml NS-B27 medium with supplements and a single NS was placed into the center of a MEA chip. Electrophysiological recording

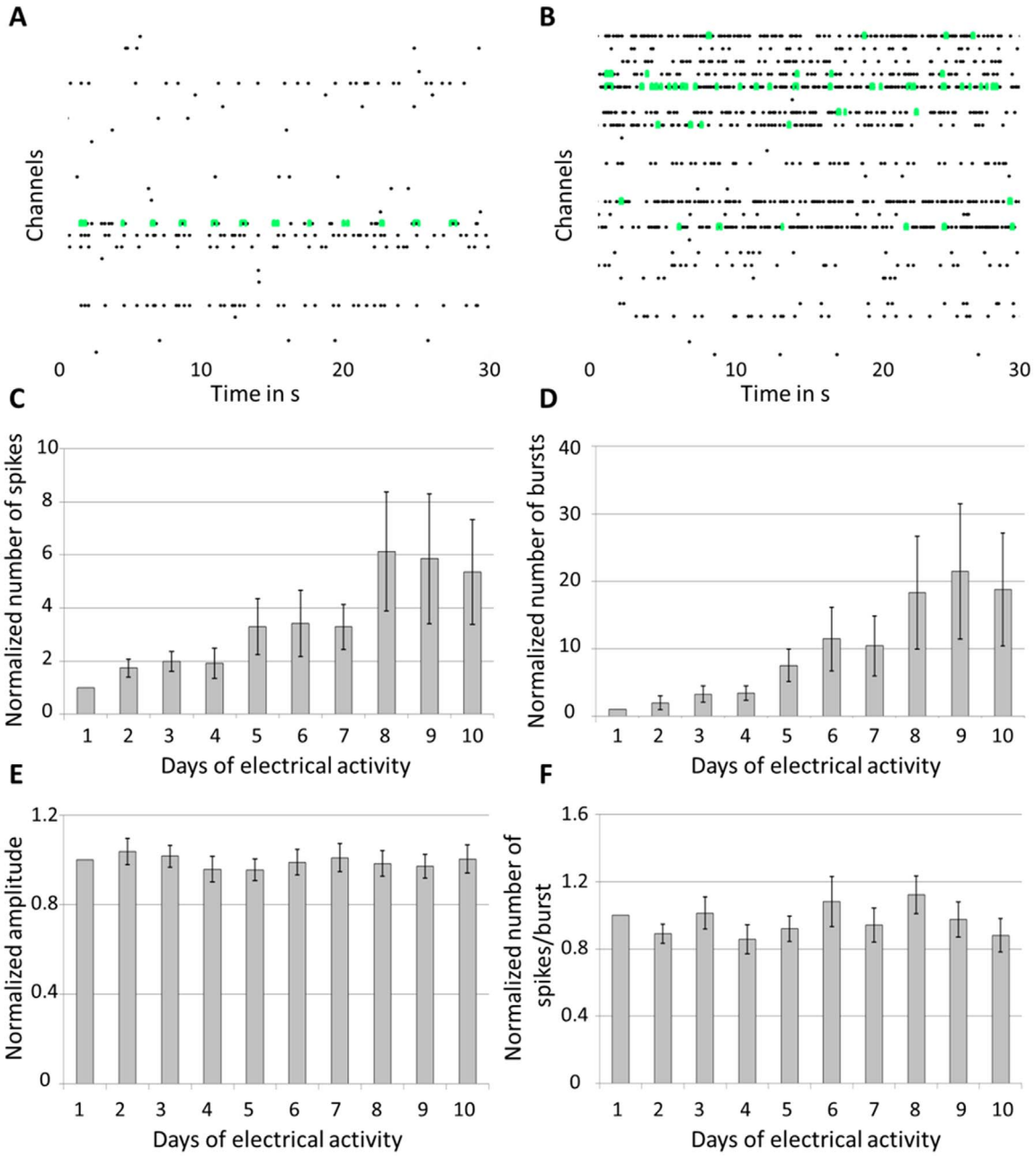

Fig. 4. Development of neuronal signaling of NS cultured on MEA chips examined over 10 days. Rasterplot showing a typical activity pattern at day 1 (A) and day 10 (B) of electrical activity. Spikes are represented by black and bursts by green bars. During the first 10 days of electrical activity, the number of spikes increased sixfold (C) and the number of bursts twentyfold (D). Further parameters such as signal amplitude (E) and number of spikes per burst (F) remained quite stable. Data are represented as mean (n = 17) ± SEM normalized to day 1. (For interpretation of the references to color in this figure legend, the reader is referred to the web version of this article.)

started 1 day later and were continued up to 21 days.

Recordings were made at a sampling rate of 10 kHz using a LabView (National Instruments, Austin, USA) programmed software (custom made). The culture temperature was kept at 37 °C using a temperature controller. A total of n = 17 NS derived from 3 independent experiments were analyzed.

2.5. Data analysis

Data analysis was performed using the MATLAB-based software tool DrCell (Nick et al., 2013). Due to low signal-to-noise ratio (SNR) of recorded data, spikes needed to be reliably separated from noise. Therefore, a novel method for spike detection in low SNR measurements was applied, combining the well-known simple threshold-based detection (Chiappalone et al., 2005; Jimbo et al., 1999) with a subsequent step that eliminates falsely detected spikes. This step is based on a new spike detection algorithm named SWTTEO (Lieb et al., 2017), which relies on the transient energy of a stationary wavelet transform (SWT). The energy is measured by an operator known as the discrete teager energy operator (TEO). A more detailed explanation of the SWTTEO algorithm can be found in the Appendix. In order to remove baseline fluctuations, raw data were preprocessed using a high-pass filter with a cut-off frequency of 50 Hz. Then, a threshold was applied to the recorded data. For each electrode the threshold was determined by multiplying the estimated standard deviation of the noise by a TCF of ± 4.5, taking negative and positive spike amplitudes into account (Nick et al., 2013). All values above (positive) or below (negative) this threshold were considered as a preselection of spikes. Subsequently, the

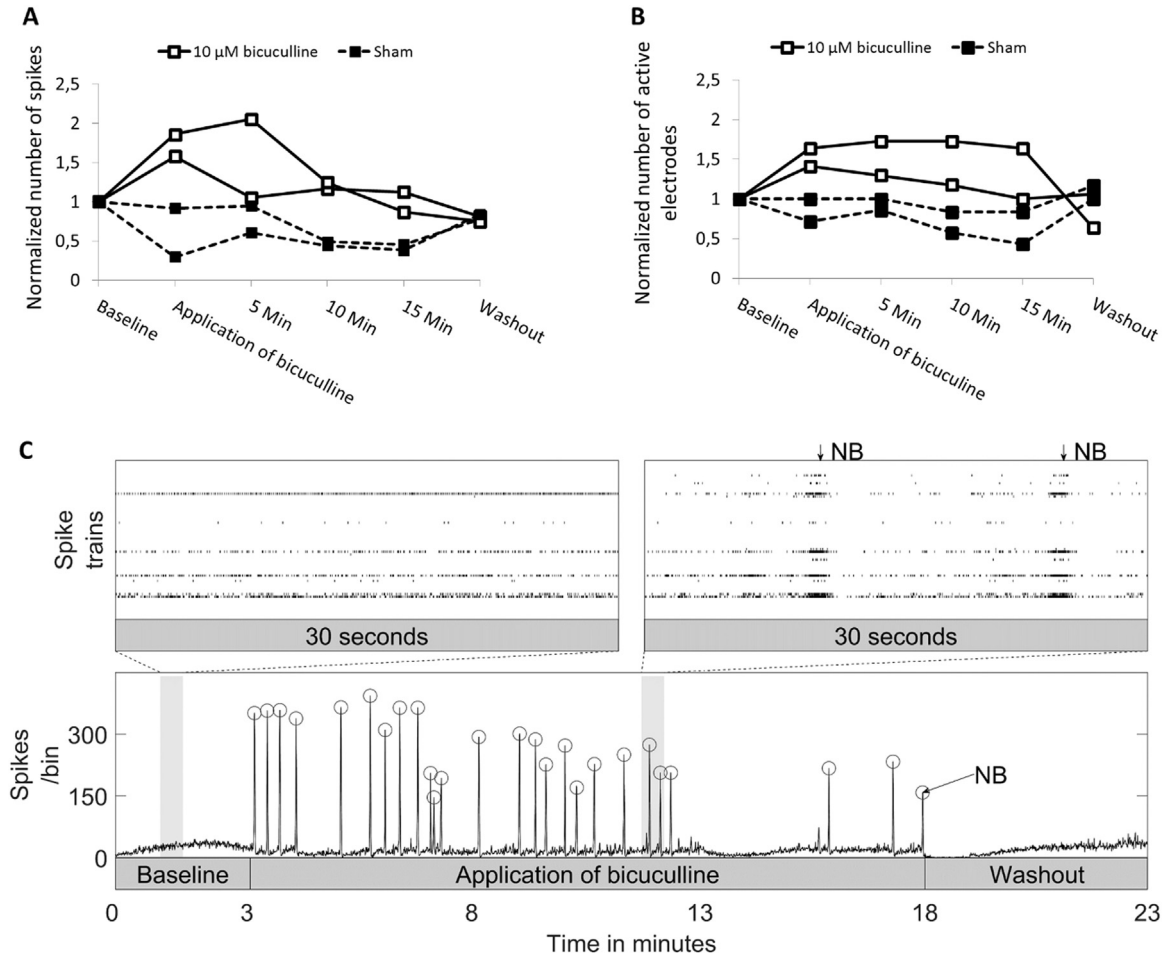

Fig. 5. Application of bicuculline results in an increased network activity with a regular pattern of NB. Immediately after bicuculline was applied to the NS, the number of spikes (A) as well as the number of active electrodes increased (B). Further, a regular pattern of NB appeared (C). After 10 min, the bicuculline induced effect weakened and after washout activity pattern returned to baseline. Data are normalized to baseline activity (n = 2).

SWTTEO algorithm was applied to the data, yielding for the corresponding electrodes the same number of spikes as detected by simple thresholding. This resulted in two independent lists with equal numbers of possible signal candidates. Finally, the intersection of the two spike lists retained only those detected by both algorithms. Based on the resulting data, active electrodes were defined as those with at least six spikes per minute (Mack et al., 2014). Further, bursts were defined as at least three spikes with inter spike intervals of less than 100 ms (Baker et al., 2006).

Moreover, to facilitate the detection of network bursts (NB, synchronous spikes recorded at multiple electrodes), the product of the number of spikes and the number of active electrodes per time bin was calculated as proposed by Chiappalone et al. (Chiappalone et al., 2005). If the product exceeded a fixed threshold, a NB was detected. In the present study a bin size of 500 ms and a threshold of 600 were used.

2.6. Pharmacological response

The pharmacological response to the GABA receptor antagonist bicuculline (10 µM in PBS) was tested for two cultures 19 days after the first signals were observed. Briefly, the medium was changed and cultures were equilibrated for 1 h. Then, the baseline activity was recorded for 3 min. Subsequently, bicuculline was applied to the cultures and signals were immediately recorded for 15 min. Thereafter, a washout with fresh NS-B27 medium with supplements was performed and activity was measured for another 5 min. Control cultures (n = 2) were treated only with PBS and processed as described above.

3. Results

3.1. Generation and characterization of hESC-derived neuronal networks

We differentiated hESC into NSC using an established differentiation protocol and further initiated the formation of three-dimensional NS. The workflow and representative images of hESC, NSC and NS are shown in Fig. 1 (upper panel). To verify the phenotype of hESC, NSC and NS immunofluorescence staining was performed (Fig. 1, lower panel). As depicted in Fig. 1B, immunostaining confirmed the presence of OCT4 and SOX2 in hESC. Likewise, an efficient differentiation of hESC to NSC occurred within seven days as reflected in Fig. 1D, *i.e.* NSC were found to be positive for SOX2 and Nestin. Concomitantly, the morphology changed (Fig. 1C, D). For further differentiation NSC were dissociated and grown in suspension culture to form three-dimensional aggregates (Fig. 1E). For quality control the diameter of the NS formed within 14 days was measured. If the average sphere diameter was about 280 µm NS were further cultured until day 18. Then, NS were placed either on coverslips for immunofluorescence staining or on MEA dish for electrophysiological recordings. NS attached and already one day after plating, outgrowing cells and neurites were observed. Cell density as well as outgrowth distance increased with time. Immunostaining against the β-tubulin$_{III}$ protein demonstrated the presence of post-mitotic neurons (Fig. 1F).

3.2. Data analysis is strongly influenced by the applied algorithms

Threshold-based spike detection in combination with SWTTEO was extensively tested on measurements of single electrodes before applying it to the whole set of experimental data. In Fig. 2A the typical activity of NS recorded by a single electrode is shown, demonstrating the critical problems for spike detection with small amplitudes and a large background noise. Fig. 2 illustrates the analysis procedure using threshold-based spike detection combined with the new algorithm SWTTEO for a typical neuronal measurement. Whenever the signal exceeds the positive or negative threshold it is considered as a preselected spike, marked with a red cross (X, Fig. 2B, C). If the SWTTEO algorithm detects the same spike (marked with a black square in Fig. 2C), this spike is kept in the spike list (marked with a green triangle). If the SWTTEO algorithm does not detect a preselected spike (Fig. 2B) it is not considered as a signal. Fig. 2D illustrates the number of detected signals as a function of TCF for threshold-based detection with (red line) or without the SWTTEO algorithm (blue line). For large TCF $\geq$ 6, both approaches detected the same number of spikes. However, differences became evident for smaller TCF. As an example, 131 spikes were detected using only threshold-based analysis with a TCF of 4.5. A subsequent evaluation with SWTTEO reduced the number to 86 indicating a reduction of false positive signals.

3.3. Electrophysiological properties of the neuronal networks

3.3.1. Spontaneous electrical activity

To characterize the functionality of the developing neuronal network the MEA platform was used as described above and data analysis was performed using threshold-based spike detection in combination with SWTTEO. Cultures were viable on the MEA dish for up to 21 days. Representative images taken 1, 4 and 10 days after plating are shown in Fig. 3 A-C.

Spontaneous electrical activity was discerned within the first week of culturing on MEA dishes or did not appear at all. Despite marked inter-sample variations in the onset of electrical activity, the activity pattern was quite similar over the first 10 days. On the subsequent days no consistent picture emerged and eventually cells detached. Thus, for further analyses only data recorded from day 1 to day 10 of electrical activity were used. First, we examined the number of active electrodes. The mean value on day 1 of electrical activity was 5.25 ± 0.59 per MEA. As displayed in Fig. 3D, this number increased about twofold over time reflecting the outgrowth of cells. Initial signals were random single spikes representing neuronal action potentials. These events were generally recorded as monophasic positive or negative as well as biphasic positive or negative spikes. Occasionally, burst-like events were seen. Fig. 4A shows a typical activity pattern on day 1 of electrical activity. At day 10 the number of spikes (small bars) as well as bursts (large bars, marked in green) was much higher as exemplarily shown in Fig. 4B. Yet, NBs were rarely detected.

The number of spikes per minute (565.75 ± 128.11 per MEA on day 1) as well as the number of burst per minute (45.69 ± 16.65 per MEA on day 1) increased over time (Fig. 4C, D). In order to facilitate a comparison of different samples data were normalized to day 1 of electrical activity. Within the first ten days after plating, the number of spikes increased sixfold and the number of bursts twentyfold. The signal amplitude hardly exceeded values of 50 µV (Fig. 4E), but occasionally also signals with amplitudes up to 100 µV were recorded by a few electrodes. The number of spikes per bursts was quite stable (4.41 ± 0.25 on day 1) showing only slight day-to-day fluctuations (Fig. 4F).

3.4. Network response to bicuculline

To examine the response of the generated NS to drugs the GABA receptor antagonist bicuculline was used. Before application of bicuculline, network activity was recorded for three minutes to determine the baseline network activity. Immediately after bicuculline was applied, the network activity increased (Fig. 5A) and signals appeared also on new electrodes resulting in an increased number of active electrodes (Fig. 5B). Furthermore, a regular pattern of NB (about 3 per minute) appeared for the first time as exemplarily shown in Fig. 5C. This activity pattern was observed for about 10 min before weakening. The activity pattern returned to baseline activity after washout indicating that this effect was reversible.

4. Discussion

hESC-derived 3D models, coupled onto microelectrode arrays, become increasingly important in the field of neurotoxicity since 2D systems differ strongly from the 3D situation *in vivo* (Frega et al., 2014). However, the SNR of extracellular recordings from 3D models is a major problem and impedes the analysis. Spike detection is typically accomplished by a threshold-based algorithm, defined by a multiple of noise's standard deviation, where TCF $\geq$ 5 were found in the literature (Frega et al., 2014; Heikkila et al., 2009; Odawara et al., 2016; Yla-Outinen et al., 2010). As a consequence, a high number of neuronal signals with small amplitudes are overseen. On the other hand, application of smaller TCF resulted in a high number of false positive results. To overcome this problem, we introduced a novel more tolerant spike detection. We detected neuronal signals with small amplitudes using a TCF of 4.5, where background noise is allowed to interfere. False positive results were subsequently excluded by a novel, robust spike detection, *i.e.* the SWTTEO algorithm (Fig. 2). In our previous studies, this new algorithm has already shown superior performance for simulated data even in a low signal-to-noise environment (Lieb et al., 2017).

In the present study it was applied for the first time to experimental data. To illustrate the influence of the analysis procedure on the number of detected signals, the exemplary measurement shown in Fig. 2A was analyzed using only threshold-based spike detection or in combination with SWTTEO (Fig. 2D). Obviously, the application of threshold-based algorithm in combination with SWTTEO resulted in a lower number of signals at TCF < 6 (*e.g.* 35% less signals using a TCF of 4.5). This decreased number was attributable to a reduction of false positive signals. The combination of these two approaches provides a more accurate analysis of neuronal signals derived from 3D cell cultures.

At present, only a limited number of groups reported on successful cultivation of neuronal 3D models on MEA chips (Frega et al., 2014; Heikkila et al., 2009; Smith et al., 2017; Yla-Outinen et al., 2010). To provide more information about the development of neuronal functionality, we carried out a detailed investigation about changes in the activity pattern of NS during the first ten days after onset of electrical activity.

In the present study, initial signals were detected within the first week after NS were placed on the MEA chip or did not appear at all consistent with data from Heikkila et al. for hESC-derived neural aggregates (Heikkila et al., 2009). Generally, initial signals were random single spikes. Occasionally, burst-like events were seen. A significant increase in the number of bursts was detected five days later (Fig. 4). Interestingly, Heikkila et al. (2009) described the occurrence of burst-events at later time points. This might be due to the different protocols for the electrophysiological measurement. In this study, single NS were placed directly on the electrode area of the MEA chips. Electrical activity was detected directly from intact 3D NS as well as from its outgrowing neurons, while Heikkila et al. (2009) analyzed only neuronal activity of the outgrowing 2D cell layer. A recent study (Frega et al., 2014) showed significant differences in the occurrence of random spikes, mean bursting and NB rate between 2D and 3D models that may explain these differences in functional development.

NB play an important role in the processing of information and in establishing appropriate neuronal connections *in vivo* (Ben-Ari, 2001; Li

et al., 2009). NB occur also in various 2D cell models (Illes et al., 2009; Odawara et al., 2016; Wagenaar et al., 2005), but unlike *in vivo* cell cultures maintain this activity pattern constant over their lifetime. The continuing presence of NB in *in vitro* may be interpreted as a developmental arrest due to missing sensory input (Wagenaar et al., 2005). It is similar to those observed *in vivo* in the absence of afferent stimuli or with acute pathologies (*e.g.* epilepsy) (Litt and Echauz, 2002; Massobrio et al., 2015). In this study, activity patterns of NS showed a distinct spiking activity along with discrete bursts that were rarely synchronized (Fig. 4B). This underlines the suitability of our 3D cultures, since they emulate *in vivo* physiology. A reduced network synchrony in neuronal 3D cell cultures was also reported for hippocampal rat neurons (Frega et al., 2014). This may be related to the GABAergic signaling. It was shown, that specific subtypes of GABA neurons have an important function in the generation of synchronized network oscillations in developing neocortex and hippocampus (Baltz et al., 2010; Ellender et al., 2010; Picardo et al., 2011). Furthermore, GABA interneurons with long-range connections seem to be involved in the development of less synchronized network activity pattern (Baltz et al., 2010; Frega et al., 2014). We hypothesize that 3D models possess more GABA interneurons with long-range connections than 2D cell cultures explaining the low network synchrony. The presence of GABA neurons in NS was confirmed by the addition of the GABA receptor antagonist bicuculline. Immediately after application, network activity increased and a regular pattern of bursts emerged that occur synchronously on different electrodes (Fig. 5). This response is physiologically reasonable and comparable to that of other cell culture models (Frega et al., 2014; Heikkila et al., 2009; Jungblut et al., 2009).

In summary, we examined electrophysiological properties of 3D hESC-derived NS using MEA technology. This platform is of high interest not only for basic research, but also for a variety of medical applications (*e.g.* transplantation, regenerative medicine) or neurotoxicological studies to verify the functionality of hESC-derived neuronal cells. In this paper, neuronal activity was analyzed using a novel method for spike detection, combining simple threshold-based algorithms with the recently introduced spike detection system SWTTEO. Using this analysis method, false positive signals are efficiently removed resulting in more accurate results compared to the simple threshold-based spike detection. We conclude that this method is highly suitable for analysis of electrical signals derived from neuronal 3D models and would be a valuable alternative to current analytical procedures.

In further studies, this novel spike detection method will be used to assess the effect of clinically relevant combinations of ionizing radiation and chemotherapy (*e.g.* anticonvulsants) on electrophysiological properties of neuronal networks.

Acknowledgments

Funding for this project was provided by the Federal Ministry of Education and Research under contract numbers 02NUK025, 02NUK034C and 03FH061PX3 and the Bavarian State Ministry for Education, Science and the Arts in the frame of ZEWIS.

Appendix A. Supporting information

Supplementary data associated with this article can be found in the online version at http://dx.doi.org/10.1016/j.bios.2017.09.034.

References

Baker, R.E., Corner, M.A., van Pelt, J., 2006. Brain Res. 1101 (1), 29–35.
Baltz, T., de Lima, A.D., Voigt, T., 2010. Front. Cell. Neurosci. 4, 15.
Ben-Ari, Y., 2001. Trends Neurosci. 24 (6), 353–360.
Birgersdotter, A., Sandberg, R., Ernberg, I., 2005. Semin. Cancer Biol. 15 (5), 405–412.
Brewer, G.J., Boehler, M.D., Ide, A.N., Wheeler, B.C., 2009. J. Neurosci. Methods 184 (1), 104–109.
Chiappalone, M., Bove, M., Vato, A., Tedesco, M., Martinoia, S., 2006. Brain Res. 1093 (1), 41–53.
Chiappalone, M., Novellino, A., Vajda, I., Vato, A., Martinoia, S., van Pelt, J., 2005. Neurocomputing 65–66, 653–662.
Colleoni, S., Galli, C., Gaspar, J.A., Meganathan, K., Jagtap, S., Hescheler, J., Sachinidis, A., Lazzari, G., 2011. Toxicol. Sci. 124 (2), 370–377.
Ellender, T.J., Nissen, W., Colgin, L.L., Mann, E.O., Paulsen, O., 2010. J. Neurosci. 30 (17), 5979–5991.
Frega, M., Tedesco, M., Massobrio, P., Pesce, M., Martinoia, S., 2014. Sci. Rep. 4, 5489.
Heikkila, T.J., Yla-Outinen, L., Tanskanen, J.M., Lappalainen, R.S., Skottman, H., Suuronen, R., Mikkonen, J.E., Hyttinen, J.A., Narkilahti, S., 2009. Exp. Neurol. 218 (1), 109–116.
Hindie, M., Vayssade, M., Dufresne, M., Queant, S., Warocquier-Clerout, R., Legeay, G., Vigneron, P., Olivier, V., Duval, J.L., Nagel, M.D., 2006. J. Cell. Biochem. 99 (1), 96–104.
Illes, S., Theiss, S., Hartung, H.P., Siebler, M., Dihne, M., 2009. BMC Neurosci. 10, 93.
Jimbo, Y., Tateno, T., Robinson, H.P.C., 1999. Biophys. J. 76, 670–678.
Johnstone, A.F., Gross, G.W., Weiss, D.G., Schroeder, O.H., Gramowski, A., Shafer, T.J., 2010. Neurotoxicology 31 (4), 331–350.
Jungblut, M., Knoll, W., Thielemann, C., Pottek, M., 2009. Biomed. Micro. 11 (6), 1269–1278.
Klein, K.L., Scott, W.J., Wilson, J.G., 1981. J. Exp. Zool. 216, 107–112.
Lepper, E.R., Smith, N.F., Cox, M.C., Scripture, C.D., Figg, W.D., 2006. Curr. Drug Metab. 7, 677–685.
Li, X., Sun, J., Chen, W., Zeng, S., Luo, Q., 2009. Proc. SPIE Int. Soc. Opt. Eng. 7176, 71760H–71767H.
Lieb, F., Stark, H.G., Thielemann, C., 2017. J. Neural Eng. 14 (3), 036013.
Litt, B., Echauz, J., 2002. Lancet Neurol. 1 (1), 22–30.
Loessner, D., Stok, K.S., Lutolf, M.P., Hutmacher, D.W., Clements, J.A., Rizzi, S.C., 2010. Biomaterials 31 (32), 8494–8506.
Luft, S., Arrizabalaga, O., Kulish, I., Nasonova, E., Durante, M., Ritter, S., Schroeder, I.S., 2017. Stem Cells Dev. 26 (5), 341–352.
Mack, C.M., Lin, B.J., Turner, J.D., Johnstone, A.F., Burgoon, L.D., Shafer, T.J., 2014. Neurotoxicology 40, 75–85.
Massobrio, P., Tessadori, J., Chiappalone, M., Ghirardi, M., 2015. Neural Plast. 2015, 196195.
Mazzoni, A., Broccard, F.D., Garcia-Perez, E., Bonifazi, P., Ruaro, M.E., Torre, V., 2007. PLoS One 2 (5), e439.
Nick, C., Goldhammer, M., Bestel, R., Steger, F., Daus, A.W., Thielemann, C., 2013. Signal Process.: Int. J. 7 (2), 96–109.
Odawara, A., Katoh, H., Matsuda, N., Suzuki, I., 2016. Sci. Rep. 6, 26181.
Picardo, M.A., Guigue, P., Bonifazi, P., Batista-Brito, R., Allene, C., Ribas, A., Fishell, G., Baude, A., Cossart, R., 2011. Neuron 71 (4), 695–709.
Pine, J., 1980. J. Neurosci. Methods 2 (1), 19–31.
Smith, I., Silveirinha, V., Stein, J.L., de la Torre-Ubieta, L., Farrimond, J.A., Williamson, E.M., Whalley, B.J., 2017. J. Tissue Eng. Regen. Med. 11 (4), 1022–1033.
Thomson, J.A., Itskovitz-Eldor, J., Shapiro, S.S., Waknitz, M.A., Swiergiel, J.J., Marshall, V.S., Jones, J.M., 1998. Sci. Transl. Med. 282 (5391), 1145–1147.
Wagenaar, D.A., Madhavan, R., Pine, J., Potter, S.M., 2005. J. Neurosci. 25 (3), 680–688.
Wagenaar, D.A., Pine, J., Potter, S.M., 2006. BMC Neurosci. 7, 11.
Weaver, V.M., Petersen, O.W., Wang, F., Larabell, C.A., Briand, P., Damsky, C., Bissell, M.J., 1997. J. Cell Biol. 137 (1), 231–245.
Willerth, S.M., Arendas, K.J., Gottlieb, D.I., Sakiyama-Elbert, S.E., 2006. Biomaterials 27 (36), 5990–6003.
Yan, Y., Shin, S., Jha, B.S., Liu, Q., Sheng, J., Li, F., Zhan, M., Davis, J., Bharti, K., Zeng, X., Rao, M., Malik, N., Vemuri, M.C., 2013. Stem Cells Transl. Med. 2 (11), 862–870.
Yla-Outinen, L., Heikkila, J., Skottman, H., Suuronen, R., Aanismaa, R., Narkilahti, S., 2010. Front. Neuroeng. 3, 111.
Zimmer, B., Lee, G., Balmer, N.V., Meganathan, K., Sachinidis, A., Studer, L., Leist, M., 2012. Environ. Health Perspect. 120 (8), 1116–1122.